AD-A183 816 A SIMPLE MOTION PLANNING ALGORITHM FOR GENERAL ROBOT MANIPULATORS(U) MASSACHUSETTS INST OF TECH CAMBRIDGE ARTIFICIAL INTELLIGENCE LAB T LOZANO-PEREZ JUN 86 1/1

UNCLASSIFIED AI-M-896 N00014-85-K-0214 F/G 12/9 NL

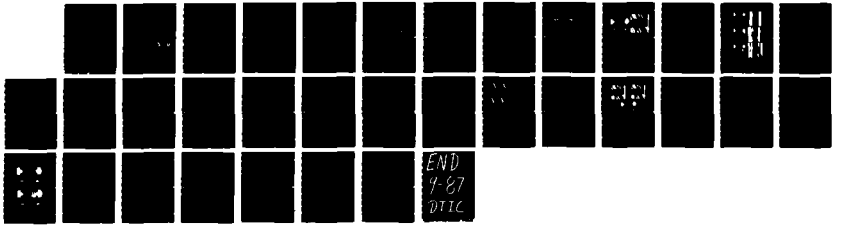

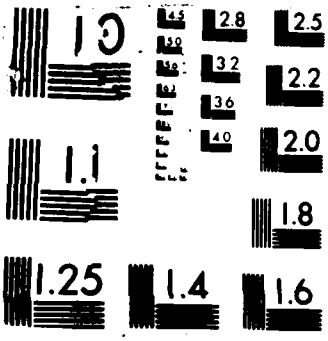
1.0
2.8
2.5
3.2
2.2
3.6
4.0
2.0
1.1
1.8
1.25
1.4
1.6

UNCLASSIFIED

SECURITY CLASSIFICATION OF THIS PAGE (When Data Entered)

(12)

REPORT DOCUMENTATION PAGE

READ INSTRUCTIONS BEFORE COMPLETING FORM

1 REPORT NUMBER	2 GOVT ACCESSION NO	3 RECIPIENT'S CATALOG NUMBER
A. I. Memo 896		

4 TITLE (and Subtitle)

A Simple Motion Planning Algorithm for General Robot Manipulators

5 TYPE OF REPORT & PERIOD COVERED

June 1986

6 PERFORMING ORG. REPORT NUMBER

7 AUTHOR(s)

Tomas Lozano-Perez

8 CONTRACT OR GRANT NUMBER(s)

N00014-85-K-0214
N00014-82-K-0334
N00014-82-K-0494

9 PERFORMING ORGANIZATION NAME AND ADDRESS

Artificial Intelligence Laboratory
545 Technology Square
Cambridge, MA 02139

10 PROGRAM ELEMENT PROJECT, TASK AREA & WORK UNIT NUMBERS

11 CONTROLLING OFFICE NAME AND ADDRESS

Advanced Research Projects Agency
1400 Wilson Blvd.
Arlington, VA 22209

12 REPORT DATE

June 1986

13 NUMBER OF PAGES

31

14 MONITORING AGENCY NAME & ADDRESS(if different from Controlling Office)

Office of Naval Research
Information Systems
Arlington, VA 22217

15 SECURITY CLASS. (of this report)

UNCLASSIFIED

15a DECLASSIFICATION/DOWNGRADING SCHEDULE

16 DISTRIBUTION STATEMENT (of this Report)

Distribution is unlimited.

17 DISTRIBUTION STATEMENT (of the abstract entered in Block 20, if different from Report)

DTIC ELECTE AUG 2 1 1987 S D CS D

18 SUPPLEMENTARY NOTES

None

19 KEY WORDS (Continue on reverse side if necessary and identify by block number)

Robotics
Motion Planning

20 ABSTRACT (Continue on reverse side if necessary and identify by block number)

This paper presents a simple and efficient algorithm, using configuration space, to plan collision-free motions for general manipulators. We describe an implementation of the algorithm for manipulators made up of revolute joints. The configuration-space obstacles for an n degree-of-freedom manipulator are spproximated by sets of n - 1 dimensional slices, recursively built up from one dimensional slices. This obstacle representation leads to an efficient approximation of the free space outside the configuration-

DD FORM 1 JAN 73 1473 EDITION OF 1 NOV 65 IS OBSOLETE
S/N 0102-014-6601

UNCLASSIFIED

SECURITY CLASSIFICATION OF THIS PAGE (When Data Entered)

20. (continued)

space obstacles.

MASSACHUSETTS INSTITUTE OF TECHNOLOGY
ARTIFICIAL INTELLIGENCE LABORATORY

A. I. Memo 896 **June, 1986**

A SIMPLE MOTION PLANNING ALGORITHM FOR GENERAL ROBOT MANIPULATORS

Tomás Lozano-Pérez

Abstract: This paper presents a simple and efficient algorithm, using configuration space, to plan collision-free motions for general manipulators. We describe an implementation of the algorithm for manipulators made up of revolute joints. The configuration-space obstacles for an n degree-of-freedom manipulator are approximated by sets of $n-1$ dimensional slices, recursively built up from one dimensional slices. This obstacle representation leads to an efficient approximation of the free space outside of the configuration-space obstacles.

Acknowledgments. This report describes research done at the Artificial Intelligence Laboratory of the Massachusetts Institute of Technology. Support for the Laboratory's Artificial Intelligence research is provided in part by a grant from the System Development Foundation, in part by the Advanced Research Projects Agency under Office of Naval Research contracts N00014-85-K-0214 and N00014-82-K-0334 and in part by the Office of Naval Research under contract N00014-82-K-0494. The author's research is also supported by an NSF Presidential Young Investigator grant.

1. Introduction

This paper presents an implementation of a new motion planning algorithm for general robot manipulators moving among three-dimensional polyhedral obstacles. The algorithm has a number of advantages: it is simple to implement, it is fast for manipulators with few degrees of freedom, it can deal with manipulators having many degrees of freedom (including redundant manipulators), and it can deal with cluttered environments and non-convex polyhedral obstacles. An examples of a path obtained from an implementation of the algorithm is shown in Figure 1.

The ability to automatically plan collision-free motions for a manipulator given geometric models of the manipulator and the task is one of the capabilities required to achieve *task-level robot programming* [15]. Task-level programming is one of the principal goals of research in robotics. It is the ability to specify the robot motions required to achieve a task in terms of task-level commands, such as "Insert pin-A in hole-B", rather than robot-level commands, such as "Move to 0.1,0.35,1.6".

The *motion-planning problem*, in its simplest form, is to find a path from a specified starting robot configuration to a specified goal configuration that avoids collisions with a known set of stationary obstacles. Note that this problem is significantly different from, and quite a bit harder than, the *collision detection* problem: detecting whether a known robot configuration or a path would cause a collision [1, 4]. Motion planning is also different from *on-line obstacle avoidance*: modifying a known robot path so as to avoid unforeseen obstacles [6, 9, 10, 11].

Although general-purpose task-level programming is still many years away, some of the techniques developed for task-level programming are relevant to existing robot applications. There is, for example, increasing emphasis among major robot users on developing techniques for off-line programming, by human programmers, using CAD models of the manipulator and the task. In many of these applications motion planning plays a central role. Arc welding is a good example; specifying robot paths for welding along complex three-dimensional paths is a time-consuming and tedious process. The development of practical motion-planning algorithms could reduce significantly the programming time for these applications.

A great deal of research has been devoted to the motion-planning problem within the last five to eight years, e.g., [2, 3, 5, 7, 8, 12, 13, 14, 16, 17, 19, 20]. But, few of these methods are simple enough and powerful enough to be practical. Practical algorithms are particularly scarce for manipulators made up of revolute joints, the most popular type of industrial robot. I know of only two previous motion-planning algorithms that are both efficient and reasonably general for revolute manipulators with three or more degrees of freedom [2, 7]. Brooks's algorithm [2] has demonstrated impressive results, but is fairly complex. Faverjon's algorithm [7], on the other hand, is appealingly simple. The basic approach of the algorithm described here is closely related to the method described by Faverjon. Many of the details of the present algorithm, however, especially the treatment of three-dimensional constraints and the free space representation, are new and more general

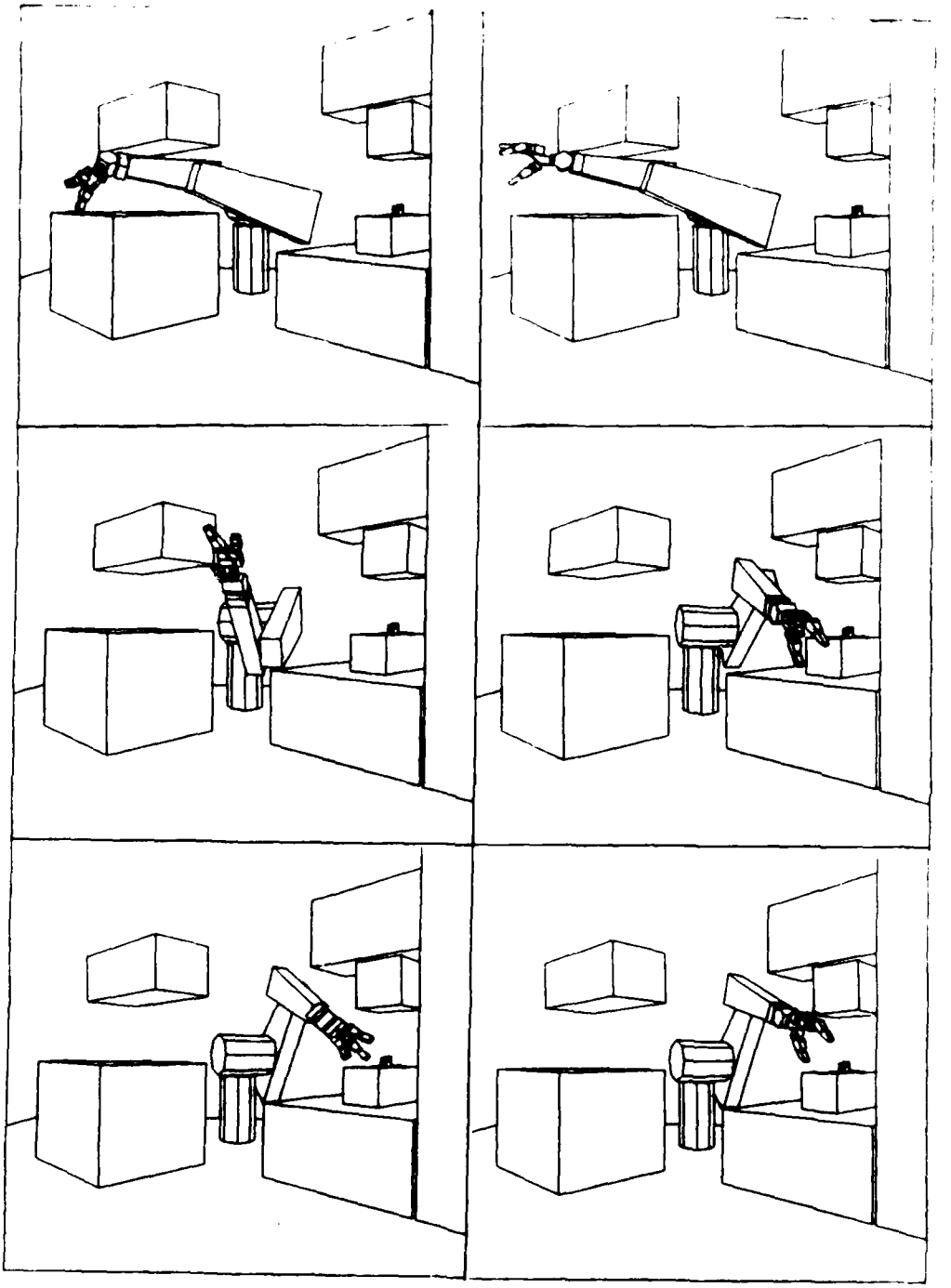

Figure 1. (a) Sample configurations along a path for all six links of a Unimation Puma manipulator obtained using the algorithm described here. The total planning time on a Symbolics 3600 Lisp Machine without floating-point hardware was 40 seconds. The incremental cost for planning another path in the same environment is approximately 2 seconds.

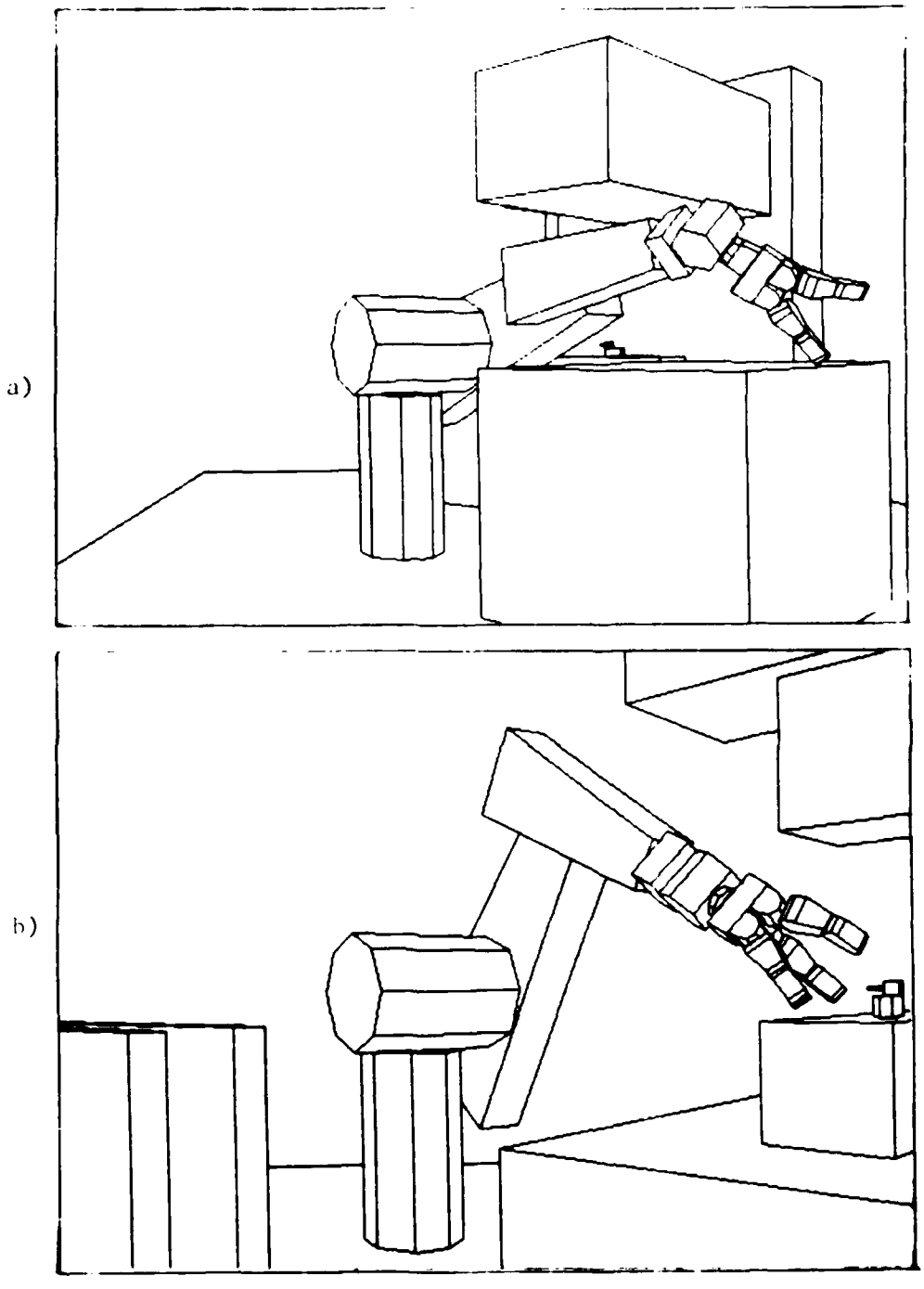

Figure 2 (a) A closeup of the initial configuration of the manipulator for the path in Figure 1b (from a different viewpoint) (b) A closeup of the final configuration of the manipulator for the path in Figure 1b. Note that the full polyhedral descriptions of the arm and end-effector are used in the algorithm

The approach taken in this algorithm is similar to that of [7, 8, 12, 13] in that it involves quantizing joint angles. It differs in this respect from exact algorithms such as [17, 19]. On the other hand, the quantization approach lends itself readily to efficient computer implementation.

The purpose of this paper is to show that motion planning for general manipulators can be both simple and relatively efficient in most practical cases. There is no reason why motion planning should be any less practical than computing renderings of three dimensional solids in computer graphics. In both cases, there are many simple numerical computations that can benefit from hardware support. In fact, it is worth noting that in the examples in Figure 1 it took longer to compute the hidden-surface displays in the figures than to compute the paths.

2. The Basic Approach: Slice Projection

The *configuration* of a moving object is any set of parameters that completely specify the position of every point on the object. *Configuration space (C-space)* is the space of configurations of a moving object. The set of joint angles of a robot manipulator constitute a configuration. Therefore, a robot's joint space is a configuration space. The cartesian parameters of the robot's end effector, on the other hand, do not usually constitute a configuration because of the multiplicity of solutions to a robot's inverse kinematics. It is possible to map the obstacles in the robot's workspace into its configuration space [3, 4, 5, 13, 14]. These *C-space obstacles* represent those configurations of the moving object that would cause collisions. *Free space* is defined to be the complement of the C-space obstacles.

Motion planning requires an explicit characterization of the robot's free space. The characterization may not be complete, for example, it may cover only a subset of the free space. But, without a characterization of the free space, one is reduced to trial and error methods to find a path. In this paper we show how to compute approximate characterizations of the free space for *simple* manipulators. By simple manipulators we mean manipulators composed of a non-branching sequence of links connected by either revolute or prismatic joints (see [18] for a treatment of the kinematics of simple manipulators). We restrict the position of link zero of a simple manipulator to be fixed. Most industrial manipulators (not including parallel-jaw grippers) are simple manipulators in this sense.

The C-space obstacles for a manipulator with n joints are, in general, n-dimensional volumes. Let C denote an n dimensional C-space obstacle for a manipulator with n joints. We represent approximations of C by the union of $n-1$ dimensional *slice projections* [13, 14]. Each $n-1$ dimensional configuration in a slice projection of C represents a range of n dimensional configurations (differing only in the value of a single joint parameter) that intersects C.

A slice projection of an n dimensional C-space obstacle is defined by a range of values for one of the defining parameters of the C-space and an $n-1$ dimensional volume. Let the $\mathbf{q} = (q_1, \ldots, q_n)$ denote a configuration, where each q_i is a joint parameter, each of which measures either angular displacement (for revolute joints) or linear displacement

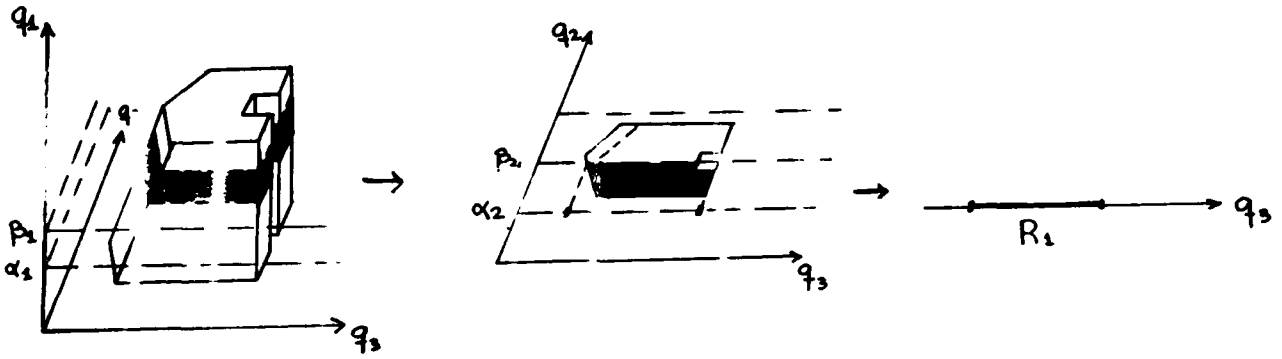

Figure 3. Slice Projection of a three-dimensional obstacle into a list of two-dimensional slices that are in turn represented by one-dimensional slices.

(for prismatic joints). Let $\{\mathbf{q} \mid q_j \in [\alpha, \beta]\}$ be the set of all configurations for which $q_j \in [\alpha, \beta]$ and let π_j be a projection operator such that

$$\pi_j(q_1, \ldots, q_n) = (q_1, \ldots, q_{j-1}, q_{j+1}, \ldots, q_n)$$

Then, the slice projection of the obstacle C for values of $q_j \in [\alpha, \beta]$ is

$$\pi_j(C \cap \{\mathbf{q} \mid q_j \in [\alpha, \beta]\})$$

The definition of slice projection is illustrated in Figure 3. In the example above, joint j above is called the *slice joint* while the other joints are known as *free joints*.

Note that a slice projection is a *conservative* approximation of a segment of an n dimensional C-space obstacle. An approximation of the full obstacle is built as the union of a number of $n-1$ dimensional slice projections, each for a different range of values of the same joint parameter (Figure 3) Each of the $n-1$ dimensional slice projections, in turn, can be approximated by the union of $n-2$ dimensional slice projections and so on, until we have a union of one dimensional volumes, that is, linear ranges. This process is illustrated graphically in Figure 3. Note that the slice projection can be continued one more step until only zero dimensional volumes (points) remain, but this is wasteful.

Consider a simple two-link planar manipulator whose joint parameters are q_1 and q_2. C-space obstacles for such a manipulator are two dimensional The one dimensional slice projection of a C-space obstacle C for $q_1 \in [\alpha, \beta]$ is some set of linear ranges $\{R_i\}$ for q_2. The ranges must be such that if there exists a value of q_2, call it ω, and a value $q_1 \in [\alpha, \beta]$, call it ζ, for which $(\zeta, \omega) \in C$, then ω is in one of the R_i (Figure 3).

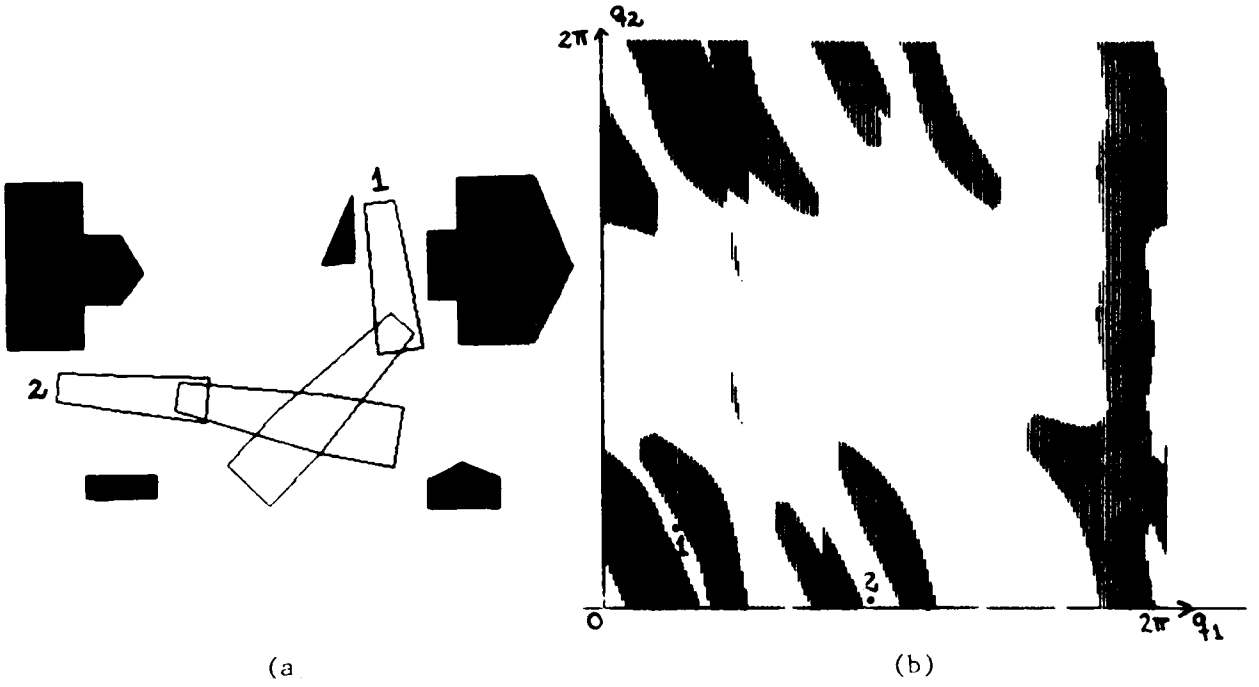

Figure 4. (a) Two link revolute manipulator and obstacles. (b) Two dimensional C space with obstacles approximated by a list of one dimensional slice projections (shown dark). The initial and final positions of the manipulator are shown in the input space and the C-space.

A representation of a configuration space with obstacles is illustrated in Figure 4b. for the two link manipulator and obstacles shown in Figure 4a. The actual configuration space is the surface of a torus since the top and bottom edge of the diagram coincide ($0 = 2\pi$), as do the left and right edge. The obstacles are approximated as a set of q_2 ranges (shown dark) for a set of values of q_1. The resolution is 2 degrees along the q_1 axis.

If the manipulator has three links, its configuration space can be constructed as follows:

1. Ignore links beyond link 1. Find the ranges of legal values of q_1 by considering rotations of link 1 around the fixed base.
2. Sample the legal range of q_1 at the specified resolution. Do steps 3 through 5 for each of the value ranges of q_1.
3. Ignore links beyond link 2. Find the ranges of legal values of q_2 by considering rotating link 2 around the positions of joint 2 determined by the current value range of q_1.

4. Sample the legal range of q_2 at the specified resolution. Do step 5 for each of these value ranges of q_2.
5. Find the ranges of legal values of q_3 by considering rotating link 3 around the position of joint 3 determined by the current value ranges of q_1 and q_2.

Some sample slices from a configuration space computed in this way can be seen in Figure 5.

Note that the process described above is an instance of a simple recursive process:

To compute C-space(i):

1. Ignore links beyond link i. Find the ranges of legal values of q_i by considering rotating link i around the positions of joint i determined by the current value ranges of $q_1, \ldots, q_{i-1}$.
2. If $i = n$ then stop, else sample the legal range of q_i at the specified resolution. Compute C-space($i + 1$) for each of these value ranges of q_i.

Observe that the basic computation to be done is that of determining the ranges of legal values for a joint parameter given ranges of values of the previous joints. This computation is the subject of Section 3.

The recursive nature of the C-space computation calls for a recursive data structure to represent the C-space. The current implementation uses a tree whose depth is $n - 1$, where n is the number of joints, and whose branching factor is the number of intervals into which the legal joint parameter range for each joint is divided (Figure 6). The leaves of the tree are ranges of legal (or forbidden) values for the joint parameter n. Many of the internal nodes in the tree will have no descendants because they produce a collision of some link $i < n$.

The main advantage of a representation method built on recursive slice projection is its simplicity. All operations on the representation boil down to dealing with linear ranges, for which very simple and efficient implementations are possible. The disadvantages are the loss of accuracy, and the rapid increase of storage and processing time with dimensionality of the C-space. Contrast this approach with one that represents the boundaries of the obstacles by their defining equations [4, 5]. Using the defining equations is cleaner and more accurate, but the algorithms for dealing with interactions between obstacle boundaries are very complex. I believe that the simplicity of slice projection outweighs its drawbacks. These drawbacks can be significantly reduced by exercising care in the implementation of the algorithms.

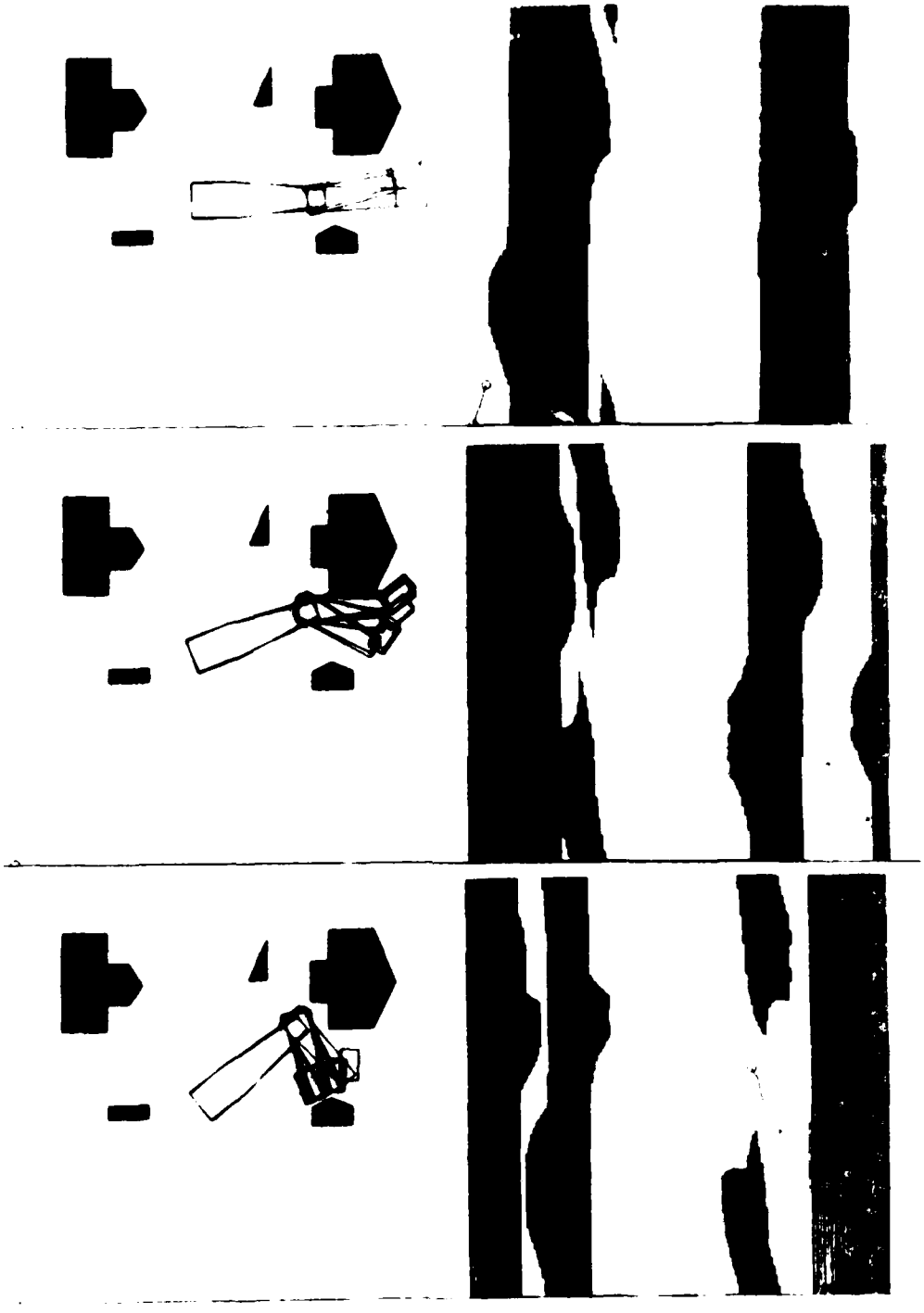

Figure 5. Three link revolute manipulator and obstacles. Samples of two dimensional slice projections used to approximate the three dimensional configuration space. Initial and final positions of the manipulator are shown in the input space and the C-space.

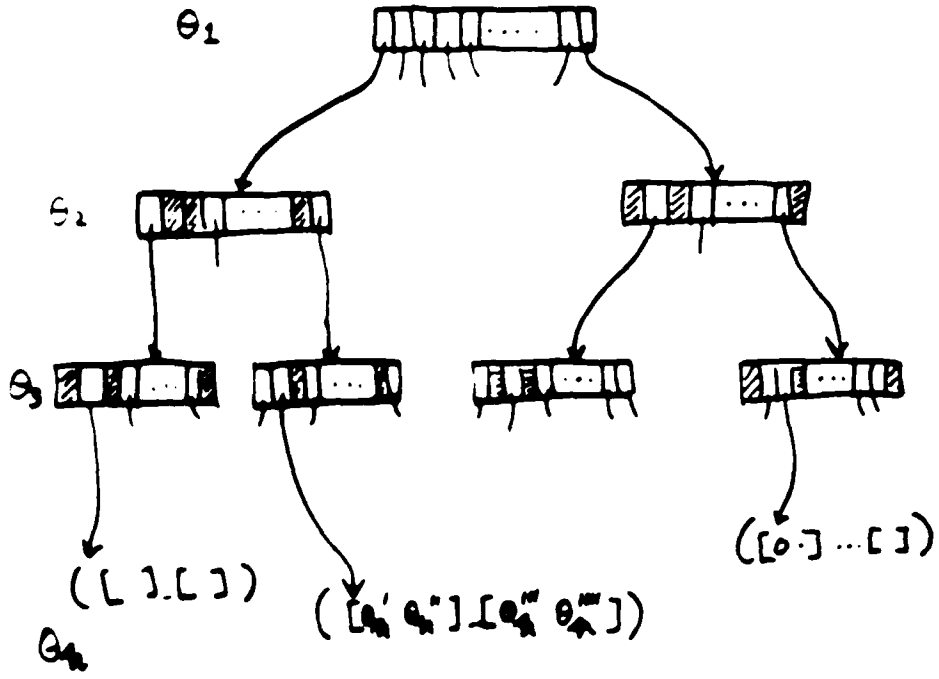

Figure 4: The recursive nature of the C-space leads to a recursive data structure: an n-level tree whose leaves represent legal ranges of configurations for the robot manipulator.

3. Slice Projections for Polygons

The key step in our approach is computing one dimensional slice projections of C-space obstacles. That is, determining the range of forbidden values of one joint parameter, given ranges of values for all previous joint parameters. We will illustrate how these ranges may be computed by considering the case of planar revolute manipulators and obstacles. We will first discuss this problem informally and then derive the solution from the equations of C-surfaces.

3.1. A geometric view

Assume that joint k (a revolute joint) is the free joint for a one-dimensional slice projection and that the previous joints are fixed at known values. Note that we assume, for now, that the previous joints are fixed at *single* values rather than *ranges* of values; we will see in Section 3.3 how to relax this restriction. We require that the configuration of the first $k-1$ links be safe, that is, no link intersects an obstacle. This is guaranteed by the recursive computation we saw in Section 2. Given these assumptions, we need to find

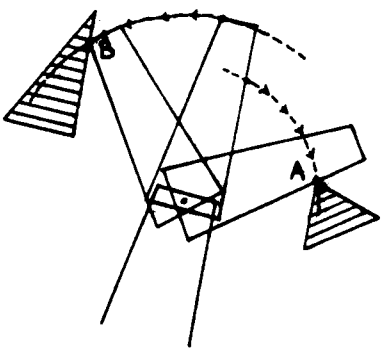

Figure 7. Contact conditions for computing one dimensional slice projections: (a) Vertex of obstacle and edge of link (b) vertex of link and edge of obstacle. The circles indicate the path of the vertices as the link rotates around the specified joint.

the ranges of values of the single joint parameter q_k that are forbidden by the presence of objects in the workspace.

The ranges of forbidden values for q_k will be bounded by angles where link k is just touching an obstacle. For polygonal links moving among polygonal obstacles, the extremal contacts happen when a vertex of one object is in contact with an edge of another object. Therefore, the first step in computing the forbidden ranges for q_k is to identify those *critical values of* q_k for which some obstacle vertex is in contact with a link edge or some link vertex is in contact with an obstacle edge (Figure 7).

The link is constrained to rotate about its joint, therefore every point on the link follows a circular path when the link rotates. The link vertices, in particular, are constrained to known circular paths. The intersection of these paths with obstacle edges determine some of the critical values of q_k, for example, B in Figure 7. As the link rotates, the obstacle vertices also follow known circular paths relative to the link. The intersection of these circles with link edges determine the remaining critical values for q_k, for example, A in Figure 7.

Determining whether a vertex and an edge segment can intersect requires first intersecting the circle traced out by the vertex and the infinite line supporting the edge to compute the potential intersection points. The existence of such an intersection is a *necessary* condition for a contact between link and obstacle, but it is not *sufficient*. Three additional constraints must hold (Figure 8): *in-edge constraint* – the intersection point must be within the finite edge segment, not just the the line supporting the edge; *orientation constraint* – the orientation of the edges at the potential contact must be compatible, that is, the edges that define the contact vertex must both be outside of the contact edge; *reachability constraint* – for non-convex objects, there must not be other contacts that prevent reaching this point.

The in-edge constraint can be tested trivially given the potential contact point and the endpoints of the contact edge. Since we know that the contact point is on the line of the edge, all that remains to be determined is whether it lies between the endpoints

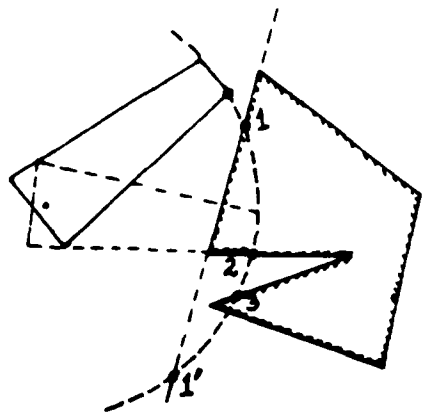

Figure 8. Given the intersection of a vertex circle and an edge line, the following conditions must be met for a feasible contact: (a) The contact must be in the edge segment, contact 1 satisfies this but $1'$ does not (b) The edges that define the contact vertex must both be outside of the contact edge, contact 1 satisfies this but contact 2 does not. (c) The contact must be reachable, contact 1 satisfies this, but contact 3 does not (this condition is only relevant for non-convex objects).

of the edge. This can be done by ensuring that the x and y coordinates of the contact point are within the range of x and y coordinates defined by the edge endpoints. Note that for contacts involving link edges and obstacle vertices, the position of the endpoints of the link edge must be rotated around the joint position by the computed value of the joint angle at the contact.

The orientation constraint can also be tested simply. All that is required is that the two edges forming the contact vertex be on the outside of the contact edge. Polygon edges are typically oriented so that they revolve in a counterclockwise direction about the boundary. Therefore, the outside of the polygon is on the right of the edge as we traverse the boundary. Given this, the feasibility of a contact can be verified simply by comparing the absolute orientations of the edges involved in the contact.

The reachability constraint, on the other hand, requires examining all the contacts of the link with a given obstacle that satisfy the first two constraints. For each contact angle q we determine whether values of q_k greater than q cause collision or whether values less than q cause collision (Section 3.2). The contact angles together with the collision directions can be merged to form the ranges of forbidden values for q_k. This process is illustrated in Figure 9.

3.2. Derivation using C-surfaces

The two types of contacts (vertex-edge and edge-vertex) give rise to the two basic type of C-space boundary (hyper-)surfaces [3, 4, 5, 14]. One type of C-surface (*type A*) characterizes the configuration of the moving object for which a vertex of the stationary obstacle is in contact with the infinite line supporting an edge of the moving object. The other (*type B*) characterizes the configuration of the moving object for which the infinite

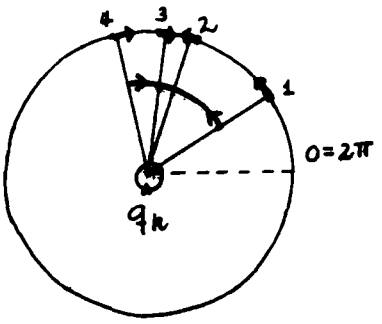

Figure 9. Constructing ranges of forbidden values using the potential contact angles and the collision directions.

line supporting an edge of the stationary obstacle is in contact with a vertex of the moving object. The equations of such surfaces are parameterized by the configuration parameters of the moving object. For planar polygons, x, y, θ can be used as configuration parameters; for manipulators, the q_i are the configuration parameters.

For a revolute joint, choose the coordinate system to be located at the joint. The coordinate representation of all of the vectors will be relative to this coordinate system. We represent a line supporting an edge by an equation of the form: $\mathbf{n}\cdot\mathbf{x}+d=0$. Where $\mathbf{n}$ is the (outward pointing) unit vector that is normal to the line and d is the perpendicular distance to the edge from the origin. The condition for a vertex $\mathbf{v}$ being in contact with such a line is simply $\mathbf{n}\cdot\mathbf{v}+d=0$.

For a type B contact, we are given a link vertex whose initial position vector (for $q_k=0$) is $\mathbf{v}$ and an obstacle edge whose line equation is $\mathbf{n}\cdot\mathbf{x}+d=0$. If the link angle is q_k, the coordinates of the rotated link vertex are:

$$\mathbf{v}' = (v_x\cos q_k - v_y\sin q_k, v_x\sin q_k + v_y\cos q_k)$$

Substituting into the plane equation yields a simple trigonometric equation in q_k (all the other terms are constant):

$$(n_x v_x + n_y v_y)\cos q_k + (n_y v_x - n_x v_y)\sin q_k + d = 0 \qquad (1)$$

From the definition of the scalar and vector product, we have that

$$n_x v_x + n_y v_y = \|\mathbf{v}\|\cos\phi, \qquad n_y v_x - n_x v_y = \|\mathbf{v}\|\sin\phi$$

where ϕ is the angle between $\mathbf{n}$ and $\mathbf{v}$. From this, it is clear that the C-surface equation is merely

$$\|\mathbf{v}\|\cos(q_k-\phi) = -d$$

The solution to this equation is:

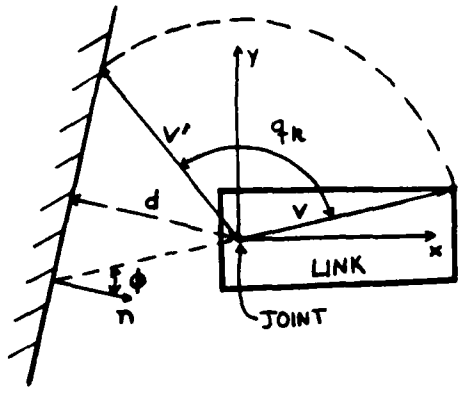

Figure 10. Illustration of terms used in (1) - (4)

$$q_k = \cos^{-1}\left(\frac{-d}{\|\mathbf{v}\|}\right) + \phi \tag{2}$$

Figure 10 illustrates this situation. There is one such C-surface for each combination of link vertex and obstacle edge. Of course, only convex vertices need be considered; no contact is possible at a concave vertex.

Using the same notation, except that the edge is a link edge and the vertex an obstacle vertex, the equation for a type A C-surface is

$$(n_x v_x + n_y v_y)\cos q_k - (n_y v_x - n_x v_y)\sin q_k + d = 0 \tag{3}$$

The only difference is the sign of the coefficient of $\sin q_k$, this arises from the fact that we are thinking of the obstacle vertex as counter-rotating while the link stands still. That is, the direction of rotation of the vertex is the opposite of q_k; this changes the sign of the sine of the angle. The solution to this equation is:

$$q_k = \cos^{-1}\left(\frac{-d}{\|\mathbf{v}\|}\right) - \phi \tag{4}$$

There is one such C-surface for each combination of (convex) obstacle vertex and link edge.

Note that there are generally two solutions to each of the equations (arising from the arccosine) since they correspond to intersections of a circle traced out by a vertex and an infinite line supporting an edge. These solutions, however, do not necessarily represent feasible contacts between the link and an obstacle. The remaining constraints illustrated in Figure 8 must also be satisfied. Of course, when the magnitude of the argument to the arccosine is greater than one, this indicates an infeasible contact, that is, the line is beyond the reach of the vertex.

The in-edge constraint can be checked, as described before, by computing the coordinates of the intersection point and the positions of the edge endpoints, given the computed values of q_k.

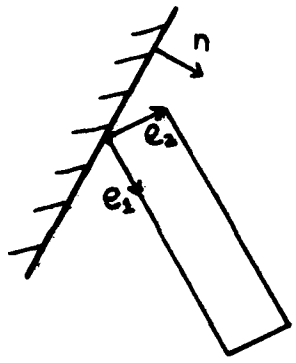

Figure 11. Testing the orientation constraint for polygonal contact

The solutions obtained from equations (2) and (4) must also satisfy the orientation constraint. One way of testing this constraint is by ensuring that the polygon edges that intersect at the contact vertex both point outward from the contact edge. If $\mathbf{e}_1$ and $\mathbf{e}_2$ are the edge vectors pointing away from the vertex (Figure 11), then the orientation constraint boils down to

$$\text{sign}(\mathbf{n} \cdot \mathbf{e}_1) \geq 0, \qquad \text{sign}(\mathbf{n} \cdot \mathbf{e}_2) \geq 0$$

where $\text{sign}(x) = x/|x|$ for $x \neq 0$ and 0 otherwise.

The reachability constraint is handled as described in Section 3.2. To do that, we must be able to tell whether an increase in q_k will move the contact away from the contact or further into contact. This can be done by computing the derivative of Eqs. (1) and (2). The left hand side of these equations is a measure of the perpendicular distance of a vertex from an edge. The sign of the derivative of this distance with respect to q_k will indicate whether a change in q_k will move further into contact or away. For example, the sign of the derivative of the distance for a type B contact (Eq. (1)) is determined by the sign of $-\sin(q_k + \phi)$ evaluated at the value of q_k that gives rise to contact.

3.3. The effect of ranges of joint angles

Our discussion thus far has been limited to situations where all the joints except the last have known fixed values. The definition of one-dimensional slice projections allows all the joints, save one free joint, to be within a range, not just a single value. We can readily convert, the slice projection problem (for ranges of joint values) to the simpler crossection projection problem (for single joint values) we have already discussed. The idea is to replace the shape of the link under consideration by the area it sweeps out when the joints defining the slice move within their specified value ranges [13, 14]. Any safe placement of the expanded link represents a range of legal displacements of the original link within the specified joint ranges.

In most cases, instead of computing the exact swept volumes, we can use a very simple approximation method. Assume the manipulator is positioned at the configuration

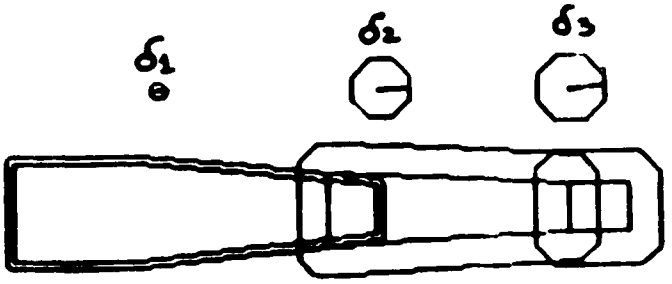

Figure 12. The k^{th} manipulator link can be grown by a radius δ_k: the maximum cartesian displacement of any point on the link in response to joint displacements ϵ_i for $i \leq k$.

defined by the midpoint of all the joint value ranges specified for the slice projection. Compute the magnitude, δ_k, of the largest cartesian displacement of any point on link k in response to any displacement within the specified range of joint values. If we "grow" each link by its corresponding radius δ_k, the grown link includes the swept area.

A polygonal approximation to the grown link can be obtained by computing the "set sum" or "Minkowski sum" of the link and a polygon enclosing a circle of radius δ [14]. An example of such an grown manipulator can be seen in Figure 12.

We can illustrate this approach by considering how to compute δ_k for a planar manipulator composed of n revolute joints. The motion of a joint affects the displacement of all subsequent links. Therefore, the maximum cartesian displacement of each link depends on the maximum total distance from any point on a link to the base joint and on the maximum angular displacement of the link. The maximum distance of points on link k is the sum of the distances between all previous joints plus the distance of any point on link k from joint k. The angular displacement of link k in a planar revolute manipulator is also the sum of the angular displacements of all the previous joints. Given the distance d and the angle θ, the magnitude of the displacement (chord of a circle) is $\sqrt{2(1-\cos\theta)}$.

Let the allowed angle range for q_k be $\alpha_k \pm \epsilon_k$; let r_k be the maximum distance of any point on link k from joint k; and let l_k be the distance from joint k to joint $k+1$. The value of δ_k is

$$\delta_k = \left[\left(\sum_{i=1}^{k-1} l_i\right) + r_k\right] \sqrt{2\left(1 - cos\left(\sum_{j=1}^{k} \epsilon_j\right)\right)}$$

Because the last link's motion is never quantized when computing the C-space, we have that: $\epsilon_k = 0$. This value of δ_k is very conservative; it is the largest displacement anywhere in the workspace. In fact, it corresponds to the displacement in a link when all the previous links are fully outstretched, that is, all the $\alpha_j = 0, j \leq k$. Different configurations would yield smaller values of δ_k.

In Figure 12 the relevant parameter values are: $\epsilon_1 = 2^o, \epsilon_2 = 2^o, \epsilon_3 = 0, l_0 = 0, l_1 = 17.0, l_2 = 17.0, r_1 = 18.44, r_2 = 17.26, r_3 = 5.385$. Therefore, the values of the δ_k are: $\delta_1 = 0.644, \delta_2 = 2.39, \delta_3 = 2.749$. Note the growth in the value of δ_k as the distance from the base increases. Because of this, one might want to choose a finer quantization for joints associated with long links near the base, for example, joint two in our example.

In some applications, if the ϵ_k are small, it may be preferable to ignore the effect of small ϵ_k during planning and simply check the resulting path for collisions. Of course, if the joint ranges ϵ_k are large, these gross approximation may be too conservative and the exact swept volume should be used.

3.4. Prismatic joints

The discussion above has concentrated on revolute joints but the approach is not limited to them. If any of the joints are prismatic, only the computation of one dimensional slices will be different and, in fact, it will be simpler.

As before, the key problem is computing the critical value of the joint parameters for which a link is in contact with an obstacle. These contacts involve contact of a vertex and an edge. So, as in the case for revolute joints, we need is determine the locus of motion of link vertices relative to obstacle edges and the locus of motion of obstacle vertices relative to link edges. For links actuated by revolute joints, we have seen that the vertices trace out circles. For links actuated by prismatic joints, the points on the link trace out lines. Potential points of contact occur where the lines defined by the motion of the vertices intersect the edges. This operation replaces the intersection of circles and lines in the preceding discussion.

The points of intersection must still satisfy the in-edge, orientation, and reachability constraints. Note that the in-edge constraint must now be modified to check, not only that the intersection point is within the finite edge segment of the polygon, but also that the contact is within the range of motion of the joint.

4. Slice Projections for Polyhedra

The basic approach described in Section 3 carries over directly to three dimensional manipulators and obstacles. There is, however, one significant difference: there are three types of contacts possible between three dimensional polyhedra. The three contact types

are: (type A) vertex of obstacle and face of link, (type B) vertex of link and face of obstacle, and (type C) edge of link and edge of obstacle.

Let us consider type B contacts first. Each revolute joint is characterized by an axis of rotation. As the joint rotates, link vertices trace circles in a plane whose normal is the joint axis. The intersection of this circle with the plane supporting an obstacle face defines two candidate points of contact (see the appendix). As in the two-dimensional case, possible contacts must satisfy three constraints to be feasible: in-face constraint - the contact must be within the obstacle face, orientation constraint - all of the link edges meeting at the vertex must be outside of the obstacle, and reachability constraint - for non-convex polyhedra, there must not be any earlier contacts that prevent reaching this one.

The in-face constraint can be checked using any of the existing algorithms for testing whether a point is in a polygon. The orientation constraint can be enforced by checking that the dot products of the face normal with each of the vectors from the contact vertex to adjacent vertices is positive [5]. The reachability constraint is enforced exactly as in the two-dimensional case by merging the forbidden angle ranges.

Type A contacts are handled analogously to type B contacts except that now the vertex belongs to an obstacle and the face to a link. The axis of rotation is still that of the manipulator joint.

Detecting type C contacts require detecting the intersection of a line (supporting a link edge) rotating about the joint axis and a stationary line (supporting an obstacle edge). The solution for this case can be found in the appendix. Of course, an intersection point must be inside both edge segments to be feasible. There is also an orientation constraint which is a bit more difficult to derive than those for type A and B contacts but not particularly difficult to check (for the derivation, see [5]).

The appendix shows the details of these computations.

5. Free Space Representation

Having obtained a conservative approximation of the C-space obstacles, the free space is simply the complement of all the obstacles. Since the obstacles are ultimately represented as sets of linear ranges, the complement is trivial to compute. A two dimensional free space, for example, will be represented as a list of one dimensional slices. Each slice represents the ranges of legal values of q_2 for some small range of values of q_1. This is in itself a reasonably convenient representation of the free space but not very compact. If we were to try to find paths through the individual slices a great deal of time would be wasted searching through nearly identical slices. A more compact representation is called for, one that captures some of the coherence between adjacent slices.

The free space representation used in the current implementation is made up of *regions*. A region is made up out of overlapping ranges from a set of adjacent slices (Figure 13). The area of common overlap of all the slices in a region is rectangular and called the region's *kernel*. In practice, we require some minimum overlap between slices in the same regions to avoid very narrow kernels.

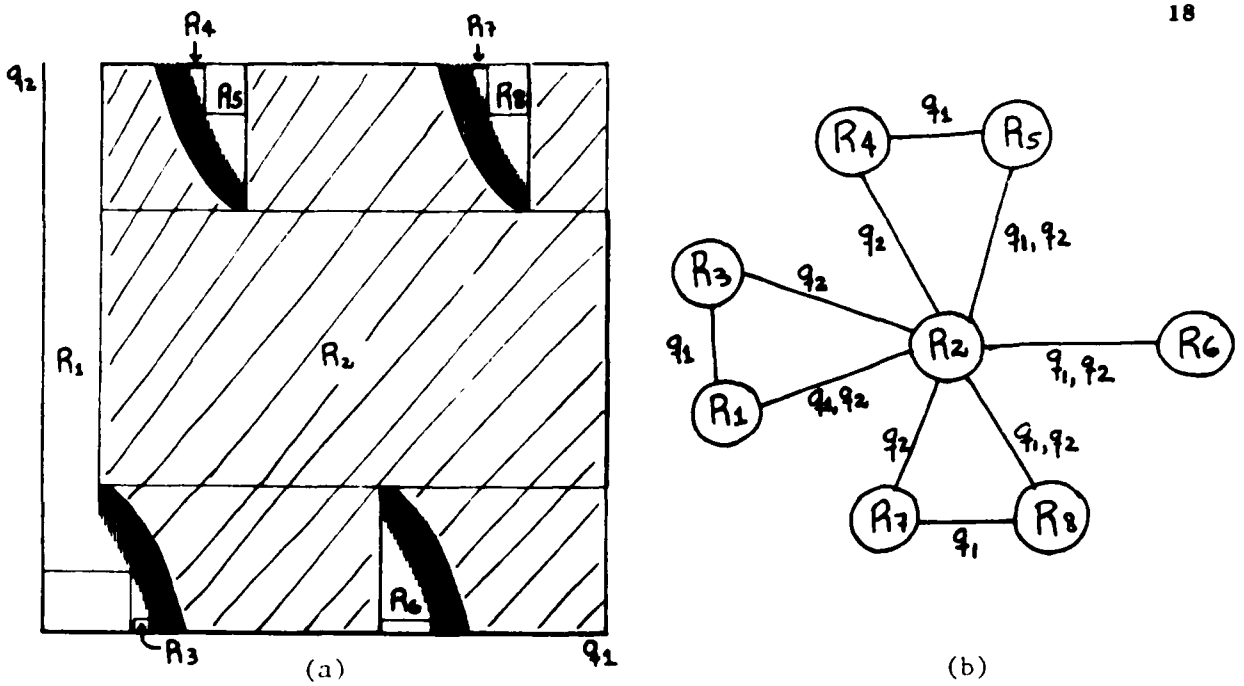

Figure 13. (a) Region definition for two link C-space. The rectangular regions are the region *kernels*. The shaded area shows region R_2. (b) Region graph corresponding to the regions in part A. The link labels indicate the existence of a common boundary in the q_1 and/or q_2 directions.

Free space regions are non-convex and so points within the region may not always be connectable by a straight line. There is, however, a simple method for moving between points within the region: move from each point along its slice to the edge of the kernel and connect these kernel points with a straight line.

To search for a path between points in different regions requires representing the connectivity of the regions. We build a ***region graph*** where the nodes are regions and the links indicate regions with common boundary. Associated with each region are a set of links to adjacent regions, each link records the area of overlap. Regions have neighbors primarily in the q_1 direction; for these neighbors, the range of q_2 values at the common region boundary is stored with the link. By construction, regions only have q_2 neighbors at the $0 = 2\pi$ boundary, anywhere else the region is bounded above and below by obstacles.

In general, each n dimensional slice is represented as a list of $n-1$ dimensional slices and one dimensional slices are a list of ranges of joint values. We have seen that two dimensional regions are constructed by joining neighboring one dimensional slice-projections. In principle, we could construct three dimensional regions by joining neighboring two dimensional regions, and so on. Instead, for three dimensional C-spaces we simply build two dimensional regions for each range of values of the first joint parameter and represent the connectivity among these regions in the region graph (Figure 14) The connectivity is determined by detecting overlap between region kernels in neighboring two dimensional slices, that is, slices obtained by incrementing or decrementing the first joint parameter. When overlap exists, the area of overlap is associated with the corre-

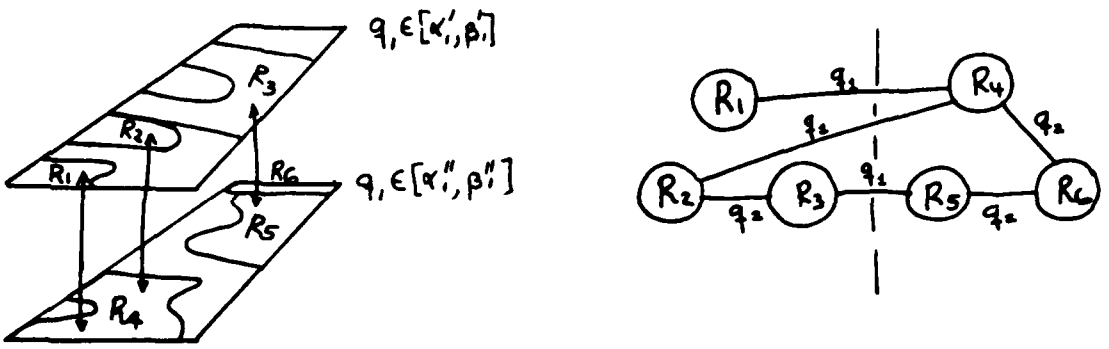

Figure 14. Region connectivity for three dimensional slices; regions can have neighbors in q_1 direction.

sponding link in the region graph. This method is readily extended to n dimensional slices by considering as neighbors slices obtained by incrementing or decrementing one of the first $n-2$ joint parameters used to define the two dimensional slice.

The main feature of this region representation is that it exploits the coherence of the free space thus, for example, it does not introduce many arbitrary divisions in the free-space such as are introduced by octree-type representations [7]. Exploiting the natural coherence has a number of practical advantages. The main result is the compactness of the representation: very few regions are required to represent rather complex free spaces. Another important result is low branching in the region graph: each region has relatively few neighbors. These characteristics of the representation also make possible some of the heuristic search technique described in section 7.

6. Searching for a Path in the Region Graph

In this section, I describe a technique for searching a region graph, This technique applies to searching any subset of the C-space; it is not necessary that the complete C-space be examined before any searching is done. Section 7 describes some heuristic strategies for limiting what parts of the C-space are actually explored.

Path searching is done by an A^* search in the region graph from the region containing the start point to the region containing the goal point. During the search, a list of search nodes is kept. Each search node is associated with some intermediate region in the region graph and represents a set of regions connecting the start region to that intermediate region. For each node, we also keep track of an *entry point* on the region boundary that represents the location where the robot path would enter the region. When a search node is expanded by extending the region path to an adjacent region, the entry point is moved to the closest point on the common boundary between the two regions. The entry point to the next region becomes the *exit point* for the current region.

To carry out the search we must associate with each search node an actual distance covered and an underestimate of the remaining distance to the goal. We use the distance

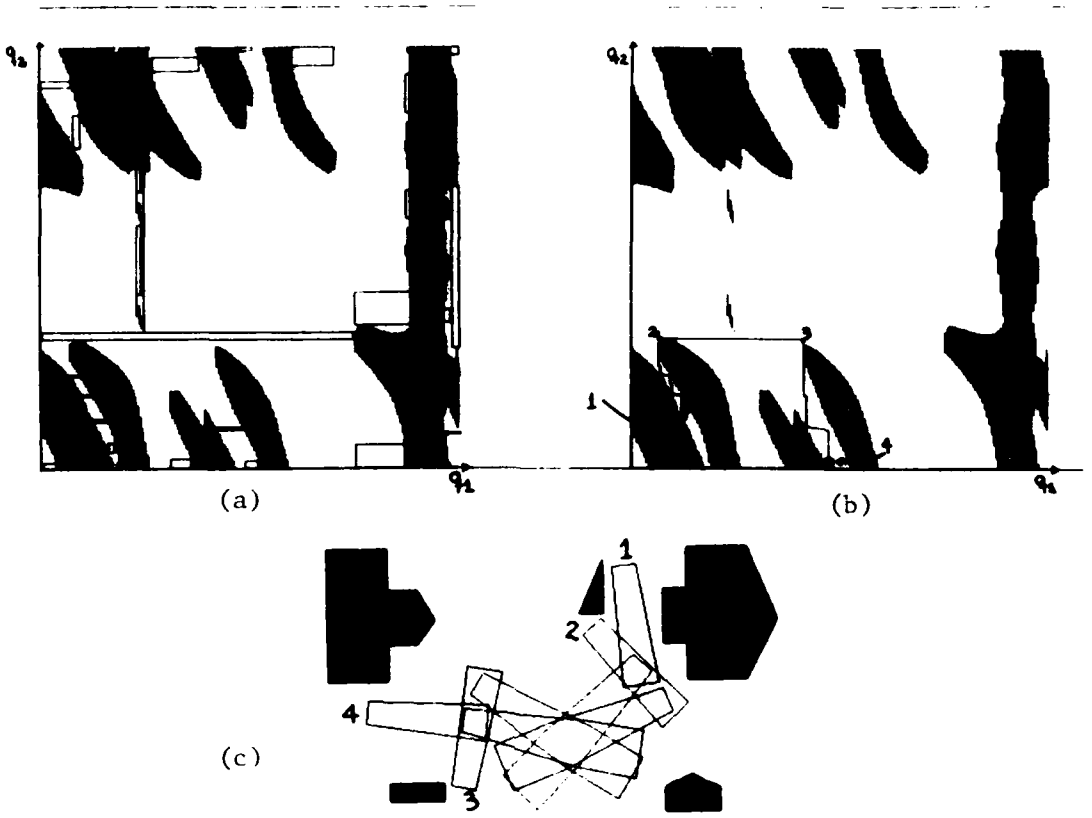

Figure 15. (a) Regions for example in Figure 4 (b) Path found between start (1) and goal (4) configurations (c) Some intermediate configurations.

between entry points to define the distance between two regions and the underestimate is the distance between the entry point and the goal. Of course, these distances are based on differences between the joint parameters modulo 2π. Once having found a list of regions connecting the start to the goal, the actual path is obtained by connecting the entry points and exit points of the regions. The entry point of the start region is the start point and the exit point of the goal region is the goal point.

A typical path found by the algorithm using the simple strategy described above is shown in Figure 15. The paths tend to be jagged: some simple postprocessing to smooth the path would be desirable and is currently under investigation. On the other hand, because of the compactness and low branching of the region representation, searching for a path tends to be very fast (less than half a second for two dimensional C-spaces)

7. Heuristic Subsets of the C-space

Having built a C-space, it may be searched repeatedly for different paths. Changes to the environment, however, will cause parts of the C-space to be recomputed. In rapidly changing environments, it may not be appropriate to compute the complete C-space since only small sections of the C-space will ever be traversed. This section describes

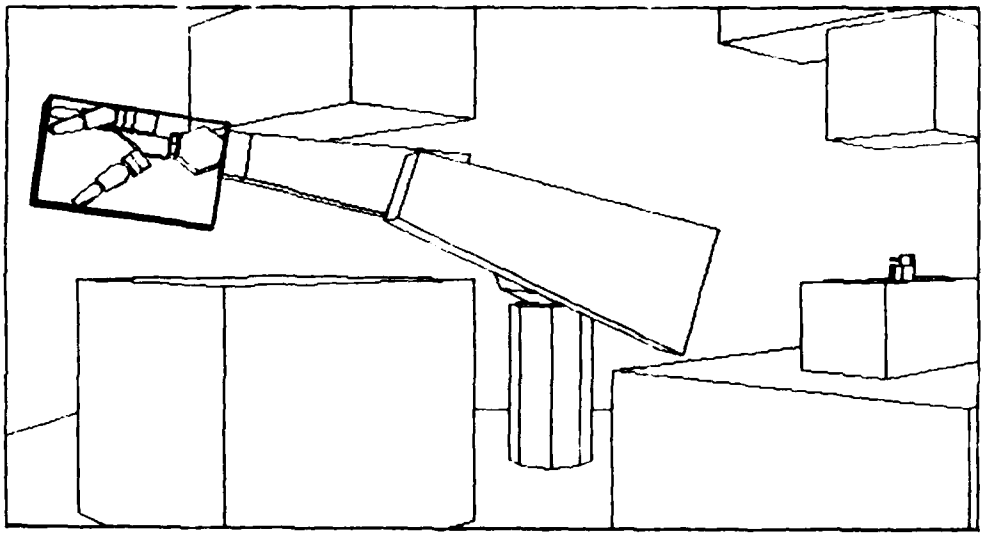

Figure 16. The first three links of the manipulator of Figure 1. The last three links and the end effector have been replaced by a simple bounding box.

experience with a number of simple heuristic strategies that help select the subset of the C-space relevant to a particular path.

7.1 Decoupling the degrees of freedom

The path shown in Figure 1 was computed using two simple heuristics to subset the C-space: First plan a path for the first 3 links and a simple conservative approximation of the rest of the manipulator (the last three links, the end-effector and the load), see Figure 16. The origin and goal for this path are chosen to be the points in free space closest to the (projection of the) actual origin and goal. Note that these points may differ from the actual origin and goal in all of the joints. Having found such a path, there remains finding paths in the six-dimensional C-space between the actual origin (resp. goal) and the origin (resp. goal) of the path. For all these paths, we compute only the portion of the C-space bounded by the joint values of the origin and goal configurations.

This strategy has the effect of nearly decoupling the degrees of freedom. The six-dimensional planning is confined to the areas near the origin and goal. Of course, this strategy will fail to find a path in the worst case, but this strategy has proven to be reliable and efficient in most practical situations.

7.2 Modifying low-dimensional paths

One alternative approach for searching for a path from configuration $(q_{s,1}, \ldots, q_{s,n})$ to configuration $(q_{g,1}, \ldots, q_{g,n})$ is the following

1. Ignore all but the first two joints. Build the free space for this reduced manipulator. Find a sequence of free space regions that contain a path from $(q_{s,1}, q_{s,2})$ to $(q_{g,1}, q_{g,2})$. Let $i = 3$.
2. Expand the portion of the free space included in the regions found so far to incorporate the link i. That is, quantize the range of values in the region and use them to compute one dimensional slice projections of the C-space for the first i links.
3. Search for a sequence of free space regions that contain a path from $(q_{s,1}, \ldots, q_{s,i})$ to $(q_{g,1}, \ldots, q_{g,i})$. If $i = n$ then stop; else increment i and go to step 2.

This strategy is illustrated graphically in Figure 17. The idea is to focus on relevant sections of the configuration space by first finding paths for successively "longer" manipulators, starting with a two-link manipulator and going all the way through to a manipulator with n links.

It is important that at each stage we consider not just a single path of the "shorter" manipulator, but a sequence of regions that span all the free-space between a set of obstacles. The addition of link n will typically change the required path for the first $n-1$ links. Therefore the search space should include more than a single path so as to avoid the need to perform a backtracking search.

This method has been implemented. The path for the four degree-of-freedom manipulator shown in Figure 18 was found by this technique. The technique leads to significant time savings on problems involving more than two degrees of freedom. Of course, since the complete configuration space is not computed, the time to plan a subsequent motion in the same workspace will be as long as that for the initial motion.

8. Discussion

The main advantages of the algorithm described here are: it is simple to implement, it is fast for manipulators with few degrees of freedom, it can deal with manipulators having many degrees of freedom including redundant manipulators, and it can deal with cluttered environments and non-convex polyhedral obstacles. The total wall-clock time to compute the C-space obstacles and then plan a path for the two-link example shown in Figure 4 and 15 is six seconds on a Symbolics 3600 Lisp Machine with floating-point operations performed in software. These times could be improved by carefully re-coding the algorithm, but they are already quite a bit faster than a human using an interactive programming system (on-line or off-line).

The main disadvantages of the algorithm are: the approximations introduced by the quantization may cause the algorithm to miss legal paths in very tight environments, and the rapid growth in execution time with the number of robot joints. This last drawback is probably inherent in any general motion planner: the worst-case time bound will be exponential in the number of degrees of freedom [19].

The performance of this algorithm shows that motion planning algorithms can be fast enough and simple enough for practical use. I believe that in many applications automatic

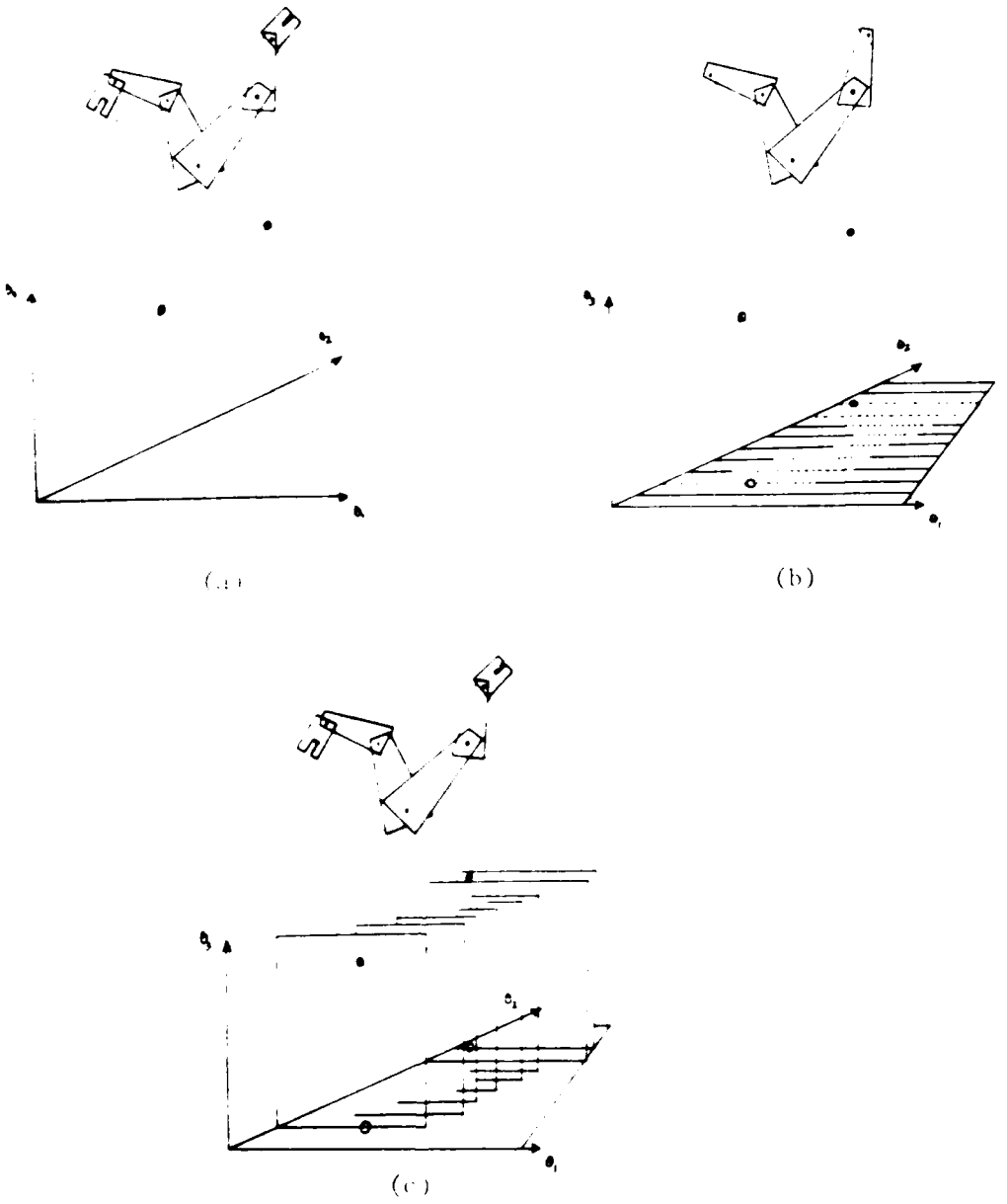

Figure 17. It is possible to alternate between searching for a path and building the C-space. (a) A three degree of freedom problem. Paths for reduced manipulators (b) limit which part of the full-dimensional C-space (c) needs to be searched.

motion planning will be more time effective than interactive off-line programming of robots. In fact, the planning times will probably be on the order of the times required to perform hidden surface elimination in graphics systems.

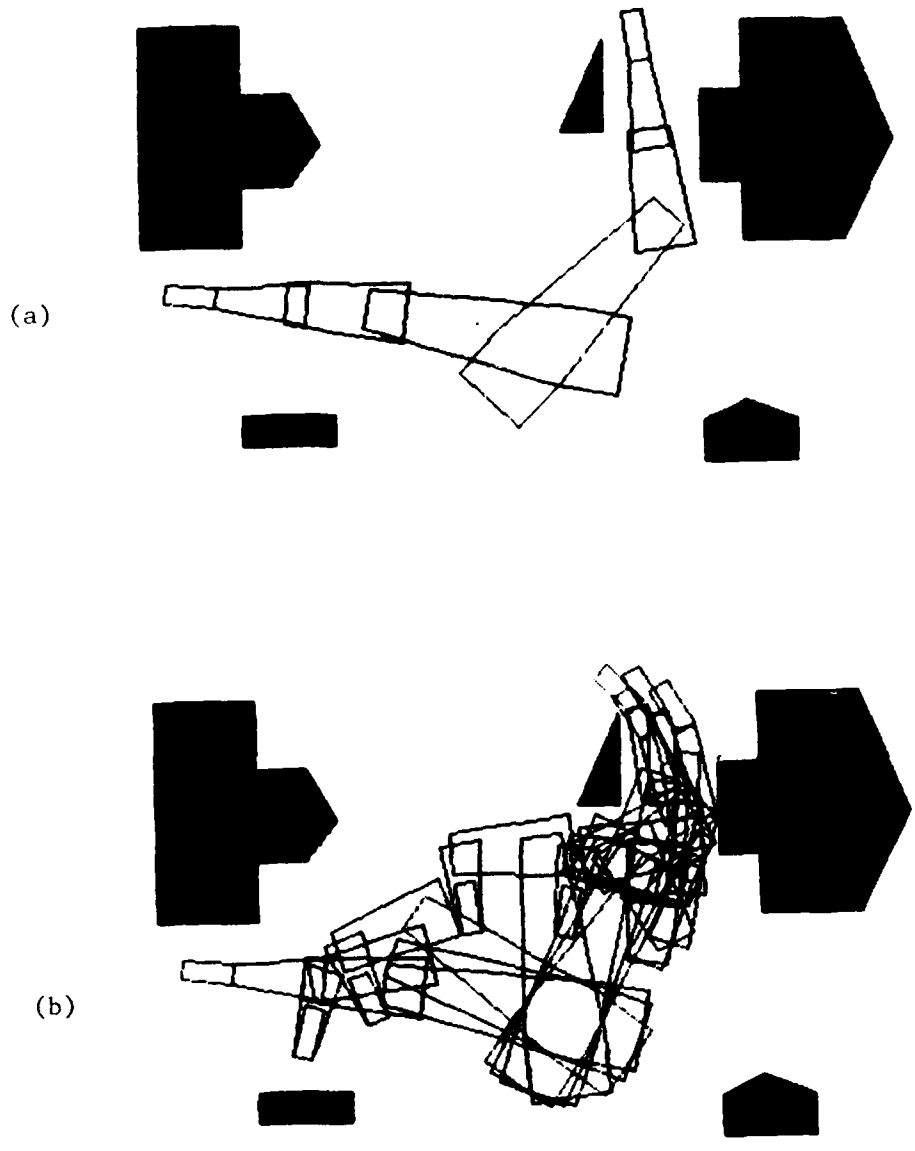

Figure 18. (a) Initial and goal configurations for a two-dimensional manipulator with four degrees of freedom. (b) Path found by the algorithm in Section 7.2.

Bibliography

1. J. W. Boyse, "Interference Detection Among Solids and Surfaces", *Comm. of ACM*, Vol. 22, No. 1, Jan. 1979
2. R. A. Brooks, "Planning Collision-Free Motions for Pick-and-Place Operations", *Intl. J. Robotics Research*, Vol. 2, No. 4, 1983.
3. R. A. Brooks and T. Lozano-Pérez, "A Subdivision Algorithm in Configuration Space for Findpath with Rotation", in Proc. Eighth Int. Joint Conf. on A. I., Aug. 1983. Also *IEEE Trans. on SMC*, Vol. SMC-15, No. 2, 224 - 233, Mar. - Apr. 1985. Also MIT AI Memo 684, Feb. 1983.
4. J. F. Canny, "Collision Detection for Moving Polyhedra", Proc. European Conf. A. I., 1984. Also MIT AI Memo 806, Oct. 1984.
5. B. R. Donald, "Motion Planning with Six Degrees of Freedom", MIT AI Tech. Rep. 791, May 1984.
6. E. Freund, "Collision Avoidance in Multi-Robot Systems", Proc. Second Intl. Symp. Robotics Research, Kyoto, August 1984. Published by MIT Press, Cambridge, Mass.
7. B. Faverjon, "Obstacle Avoidance Using an Octree in the Configuration Space of a Manipulator", Proc. IEEE Intl. Conf. Robotics, Atlanta, March 1984.
8. L. Gouzenes, "Strategies for Solving Collision-Free Trajectory Problems for Mobile and Manipulator Robots", *Intl. J. Robotics Research*, Vol. 3, No. 4, 1984.
9. N. Hogan, "Impedance Control: An Approach to Manipulation", Amer. Control Conf., June 1984.
10. O. Khatib and J. F. Le Maitre, "Dynamic Control of Manipulators Operating in a Complex Environment", Proc. Third CISM-IFToMM, Udine, Italy, Sept. 1978.
11. B. H. Krogh, "Feedback Obstacle Avoidance Control", Proc. 21st Allerton Conf., Univ. of Ill., Oct. 1983.
12. C. Laugier and F. Germain, "An Adaptive Collision-Free Trajectory Planner", Proc. Int. Conf. Adv. Robotics, Tokyo, Sept. 1985.
13. T. Lozano-Perez, "Automatic Planning of Manipulator Transfer Movements", *IEEE Trans. on SMC*, Vol. SMC-11, No. 10, 681 - 698, Oct. 1981. Also MIT AI Memo 606, Dec. 1980.
14. T. Lozano-Pérez, "Spatial Planning: A Configuration Space Approach", *IEEE Trans. on Computers*, Vol C-32, No. 2, 108 - 120, Feb. 1983. Also MIT AI Memo 605, Dec. 1980.
15. T. Lozano-Perez, "Robot Programming", *Proceedings of the IEEE*, Vol 71, No. 7, 821 - 841, July 1983. Also MIT AI Memo 698, Dec. 1982.
16. T. Lozano-Pérez and M. A. Wesley, "An Algorithm for Planning Collision-Free Paths Among Polyhedral Obstacles", *Comm. of the ACM*, Vol. 22, No. 10, 560 - 570, October 1979.
17. C. O'Dúnlaing, M. Sharir, and C. K. Yap, "Retraction: A New Approach to Motion Planning", *15th ACM STOC*, 207 - 220, 1983.
18. R. P. Paul, *Robot Manipulators*, MIT Press, 1981.

19. J. Schwartz and M. Sharir, "On the Piano Mover's Problem II", Courant Inst. of Math. Sci. Tech. Rep. 41, Feb. 1982.

20. S. Udupa, "Collision Detection and Avoidance in Computer Controlled Manipulators", Proc. Fifth Intl. Joint Conf. AI, Cambridge, 1977.

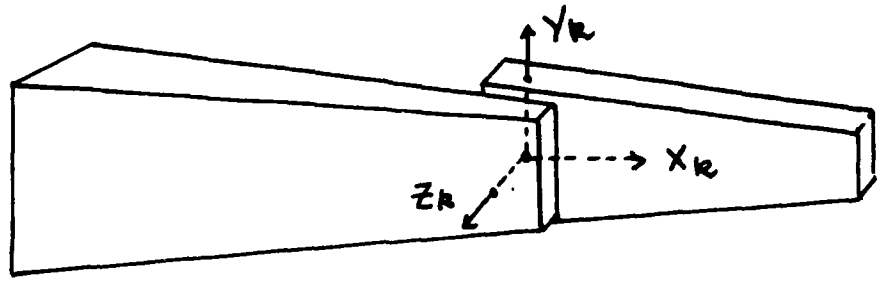

Figure 19. Joint coordinate system.

Appendix: Computing contact angles for polyhedra

In what follows we assume that we are dealing with a convex polyhedron describing link k and an obstacle polyhedron (not necessarily convex). The coordinate system is chosen so that the origin corresponds to the position of revolute joint k and the z axis is aligned with the joint axis (Figure 19). The coordinate representation of all vectors is relative to this coordinate system. We assume that the initial position of the link polyhedron corresponds to $q_k = 0$. We are interested in computing values of q_k for which the link is in contact with the obstacle polyhedron.

Type B contact: vertex of link and face of obstacle

We are given a vertex of the link whose position vector is $\mathbf{v}$ and an obstacle face whose plane equation is $\mathbf{n} \cdot \mathbf{x} - d = 0$ ($\mathbf{n}$ is the plane's outward-facing unit normal). We solve for the angle q_k that rotates the vector onto the plane. We obtain the equation for q_k by substituting the vertex's position, rotated by q_k, into the plane equation and solving for q_k.

The coordinates of the position vector for the rotated vertex are:

$$\mathbf{v}' = (v_x \cos q_k - v_y \sin q_k, v_x \sin q_k + v_y \cos q_k, v_z)$$

Substituting into the plane equation yields $\mathbf{n} \cdot \mathbf{v}' - d = 0$, this yields a simple trigonometric equation

$$(n_x v_x + n_y v_y) \cos q_k + (n_y v_x - n_x v_y) \sin q_k = -d - n_z v_z \tag{5}$$

whose solution is Eq. (6).

$$q_k = \cos^{-1}\left(\frac{-n_z v_z - d}{\sqrt{(v_x^2 + v_y^2)(1 - n_z^2)}}\right) + \operatorname{atan}(n_y v_x - n_x v_y, n_x v_x + n_y v_y) \tag{6}$$

Eq. (5) is the equation for a type B C-surface [14]. Note that if we let $n_z = 0$, then Eq. (5) and Eq. (1) are essentially identical. The arctangent simply computes the angle

between the plane normal and the projection of $\mathbf{v}$ on the xy plane; this magnitude is analogous to ϕ in the planar case. Eq. (6) and Eq. (2) are also related in the same way.

The left hand side of the Eq. (5) represents the perpendicular distance of the rotated vertex from the obstacle plane. The sign of the derivative of this quantity with respect to q_k can be used to determine whether increasing or decreasing q_k causes a collision.

The orientation constraint simply requires testing whether the other endpoint of all the edges meeting at the contact vertex are *on the outside* of the plane. This is done by substituting the position vector of these endpoints into the left hand side of the plane equation and testing that the value is positive.

Type A contact: vertex of obstacle and face of link

We are given an obstacle vertex whose position vector is $\mathbf{v}$ and a link face whose plane equation is $\mathbf{n} \cdot \mathbf{x} + d = 0$ ($\mathbf{n}$ is the plane's outward-facing normal). The solution for q_k is almost identical to the type A case, the only difference is the sign of the first argument to the arctangent. This reflects the fact that in type A contact we are treating the link as stationary and assuming the object is rotating *in the opposite direction*. This changes the sign of the sine of the angle.

Type C contact: edge of obstacle and edge of link

This case is substantially more difficult; we follow the derivation in [1]. We represent points on the edges parametrically in t. Therefore, points on the link's edge are represented by $t_l\mathbf{m} + \mathbf{v}$ where $\mathbf{v}$ is the position vector of one of the endpoints of the edge and $\mathbf{m}$ is a vector along the edge (actually the difference vector between the endpoints). The parameter $t_l \in [0, 1]$ parameterizes position along the edge. We can represent the vector along the obstacle edge similarly as $t_o\mathbf{n} + \mathbf{w}$ for $t_o \in [0, 1]$.

As the edge rotates around the z axis, points on the edge trace out circles. The equation for points on those circles are:

$$x^2 + y^2 = (m_x t_l + v_x)^2 + (m_y t_l + v_y)^2$$
$$z = m_z t_l + v_z$$

These can be combined by solving the second equation for $t_l = \frac{z - v_z}{m_z}$ and substituting into the first to obtain:

$$x^2 + y^2 = \left(\frac{m_x}{m_z}(z - v_z) + v_x\right)^2 + \left(\frac{m_y}{m_z}(z - v_z) + v_y\right)^2 \tag{7}$$

This is an implicit equation for points on the rotation surface.

The parametric form of the obstacle edge can be used to solve for the intersection of the edge with the rotation surface.

$$x = n_x t_o + w_x, \qquad y = n_y t_o + w_y, \qquad z = n_z t_o + w_z$$

Substituting into Eq. (7) gives a quadratic equation in t_o.

Define the following terms:

$$p = (n_x^2 - n_y^2)m_z^2 - (m_x^2 + m_y^2)n_z^2$$
$$q = 2[(n_x w_x - n_y w_y)m_z^2 - (m_x^2 + m_y^2)(w_z - v_z)n_z - (m_x v_x + m_y v_y)m_z n_z]$$
$$r = (w_x^2 - w_y^2)m_z^2 - [(m_x(w_z - v_z) + v_x m_z)^2 + (m_y(w_z - v_z) + v_y m_z)^2]$$

The quadratic equation that must be solved for t_o is

$$pt_o^2 + qt_o + r = 0$$

Having t_o we can solve for t_l since we know that the z values at contact must be equal. Therefore,

$$t_l = \frac{n_z t_o + w_z - v_z}{m_z}$$

Given values for t_l and t_o, we must first check that they are in the range $[0, 1]$ (the in-edge constraint), then we can compute points of intersection on each of the edges. Let $\mathbf{l}$ be the position vector of the intersection point on the link edge and $\mathbf{o}$ the position of the intersection point on the object edge. Then,

$$q_k = \text{atan}(l_x o_y - l_y o_x, l_x o_x + l_y o_y)$$

Note, however, that we have assumed, when deriving Eq. (7) that $m_z \neq 0$. In the not uncommon event that it is, then all the points on the rotation surface have $z = v_z$ and so will the intersection point with the obstacle edge. We can use this to obtain $t_o = \frac{v_z - w_z}{n_z}$. We can then solve for t_l by using the fact that the contact point on the link edge will be on the same circle as the contact point on the obstacle edge:

$$(m_x t_l - v_x)^2 + (m_y t_l - v_y)^2 = (n_x t_o - w_x)^2 + (n_y t_o - w_y)^2$$

But we know the value of t_o so this is a quadratic equation for t_l. Given the values of t_l and t_o we can solve for q_k as above.

In addition to solving for the value of the contact angle we must compute the derivative of the distance to the contact as a function of q_k. As before, this will determine whether the contact angle is a potential upper or lower bound for a contact range. Unfortunately, this is not as simple as it is for type A and B contacts.

When the two edges are in contact, any motion component perpendicular to both of them will cause a collision while a component of motion along either edge will not cause a collision. The direction perpendicular to both edges is simply the cross product of the two edge vectors (given the link edge rotated to the contact angle):

$$\mathbf{c}(q_k) = \mathbf{m}(q_k) \times \mathbf{n}$$

The q_k dependence has been indicated explicitly.

One problem here is that we do not know whether $\mathbf{c}$ is outward pointing or not. We can decide that by dotting $\mathbf{c}$ with a direction known to point into the link. If $\mathbf{e}_1$ and $\mathbf{e}_2$ are the direction vectors of edges meeting the link edge at one of its vertices (see Figure

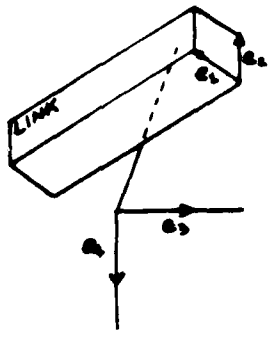

Figure 20. The definition of the $\mathbf{e}_i$ for $i = 1, 2, 3, 4$

20), then $\mathbf{e}_1 + \mathbf{e}_2$ is a direction pointing into the link volume. Let $k = \text{sign}(\mathbf{c} \cdot (\mathbf{e}_1 + \mathbf{e}_2))$, then $k\mathbf{c}$ is the outward-pointing normal we require (see [5] for a careful derivation).

Given the value of k, the type C C-surface equation can be written as [14]:

$$k\mathbf{c}(q_k) \cdot (\mathbf{w} - \mathbf{v}(q_k)) = 0 \tag{8}$$

Differentiating the left hand side with respect to q_k yields

$$((w_y m_x - w_x m_y)n_z + (d_z m_x - v_x m_z)n_y - (d_z m_y - v_y m_z)n_x)k \sin q_k +$$
$$((w_y m_y + w_x m_x)n_z + (d_z m_y - v_y m_z)n_y - (d_z m_x - v_x m_z)n_x)k \cos q_k$$

where $d_z = v_z - w_z$. If this derivative is negative then increasing q_k will cause a collision.

We are not done yet. We must guarantee that the contact satisfies the orientation constraint. The following are necessary and sufficient conditions for this [5]:

$$s = \text{sign}(\mathbf{c} \cdot \mathbf{e}_1) = \text{sign}(\mathbf{c} \cdot \mathbf{e}_2)$$
$$s' = \text{sign}(\mathbf{c} \cdot \mathbf{e}_3) = \text{sign}(\mathbf{c} \cdot \mathbf{e}_4)$$
$$s \neq s'$$

These conditions are analogous to the type A and B cases.

Although the derivation of the type C case is a bit involved, the actual amount of computation involved is not large.

END

9-87

DTIC